BUTTERWORTH HEINEMANN

Polymer Vol. 36 No. 20, pp. 3809–3817, 1995

0032-3861/95/$10.00+0.00

Rheo-optical investigation of a polystyrene melt

H. U. Hoppler, A. Dinkel and I. Tomka*
Eidgenössische Technische Hochschule, Institut für Polymere, CH-8092 Zürich, Switzerland
(Received 9 June 1994; revised 25 August 1994)

The transient birefringence and the transient tensile stress of a polystyrene melt at 140°C elongated with constant stretch rate ($\dot{\lambda}$) and constant Hencky strain rate ($\dot{\epsilon}$) are presented. Compared with the response during linear viscoelastic deformation, the values of the reduced birefringence and the reduced stress are higher when the elongation is performed with $\dot{\epsilon} = \text{const.}$, and are lower when the elongation is carried out with $\dot{\lambda} = \text{const.}$. The stress-optical coefficient turns out to be a function of duration and rate of deformation.

(Keywords: flow birefringence; simple elongation; polystyrene melt)

INTRODUCTION

This work deals with the orientational behaviour of molten polystyrene (PS) in elongational flows with exponentially and linearly increasing extension ratios. During deformation, birefringence $\Delta n(t)$ was observed as a measure of the molecular orientation by means of a newly developed instrument. In polymer melts and amorphous solid polymers (such as atactic PS), the birefringence is due to the orientation of optically anisotropic chain segments, which are generally considered to have cylindrical symmetry. To characterize molecular orientation in such systems, the second moment of the segmental orientation distribution function, the so-called Hermans orientation function f_H, may be used[1,2]:

$$f_H = \tfrac{1}{2}\langle 3\cos^2\theta - 1\rangle \tag{1}$$

Here θ is the angle between the draw direction and the optical axis of the segment. With this function, the birefringence during elongation can be written as[1,2]:

$$\Delta n(t) = f_H \Delta n_{max} \tag{2}$$

where Δn_{max} is the maximum or intrinsic birefringence of the system. For PS, Δn_{max} is reported[3–7] to be -0.1 ± 0.05.

We selected atactic PS for the investigation, because: (i) it reveals pronounced rheo-optical effects due to its comparatively high stress-optical coefficient[8]; and (ii) it contains only linear molecules[9], so that complications due to chain branching will not occur.

Elongation has been chosen as the type of deformation, for the following reasons: (i) Elongation flows are simple in concept[10]. The principal axes of stress, strain and optical anisotropy all coincide and do not change their orientation during deformation. For an initially isotropic sample, the change of symmetry due to a simple elongation is[11] $K_h \rightarrow D_{\infty h}$ ($D_{\infty h}$ is also called fibre symmetry or transverse isotropy). During and after deformation, the principal components of any property $\boldsymbol{a}$ that is represented by a second-rank tensor are:

$$a_I \neq a_{II} = a_{III}$$

(ii) Large homogeneous deformations which yield physical properties with strong anisotropy can be rather easily performed by means of a rheometer with rotary clamps[12,13].

The intentions of this work are as follows:

(i) To investigate the development of the transient birefringence $\Delta n(t)$, i.e. the orientational behaviour, of PS during simple elongation at constant stretch rate $d\lambda_I/dt = \text{const.}$ and at constant Hencky strain rate $d\epsilon_I/dt = d(\ln\lambda_I)/dt = \text{const.}$. Zülle *et al.*[14] showed the response of a polymer melt (low-density polyethylene (LDPE) at 150°C) was 'thinning' when the first principal extension ratio λ_I increased constantly and 'hardening' when λ_I increased exponentially with time, both in elongation and in shear. The terms 'hardening' and 'thinning' mean that the viscosity increases above the linear viscoelastic response or stays below it. If the material is considered to be incompressible, then the two types of flow are characterized by:

$$\dot{\epsilon}_I(t) = \dot{\epsilon}_0 h(t) \qquad \dot{\epsilon}_{II}(t) = \dot{\epsilon}_{III}(t) = -0.5\dot{\epsilon}_I(t) \tag{3a}$$

$$\dot{\lambda}_I(t) = \dot{\lambda}_0 h(t) \qquad \dot{\lambda}_{II}(t) = \dot{\lambda}_{III}(t) = [\dot{\lambda}_I(t)]^{-1/2} \tag{3b}$$

where $\dot{\epsilon}_0$ and $\dot{\lambda}_0$ are constants and $h(t)$ is the unit step function. Analogous to the viscosity, we define for these flows, which are often designated as strong and weak, two optical functions. The strong reduced birefringence is:

$$\Delta n_s = \Delta n(t)/\dot{\epsilon}_0 \tag{4}$$

and the weak reduced birefringence is:

$$\Delta n_w = \Delta n(t)/\dot{\lambda}_0 \tag{5}$$

* To whom correspondence should be addressed

(ii) To investigate the time dependence of the stress-optical coefficient (*SOC*):

$$C(t) = \Delta n(t)/\sigma(t) \qquad (6)$$

i.e. the ratio of the transient birefringence and the transient tensile stress. The rheo- or stress-optical law requires that the *SOC* of a polymer melt is constant, as long as the stress is below 1 MPa[8,15]. However, there is experimental[16] and theoretical[17,18] evidence that the *SOC* of a polymer melt is not a constant. Furthermore, two authors of the present work recently proposed a kinetic orientation model for polymer melts which predicts that the *SOC* is a function of time, even in the linear viscoelastic range of deformation[19].

EXPERIMENTAL

Sample preparation and characterization

The material investigated was a commercial, atactic polystyrene homopolymer: Standard-Polystyrol 158 K. The pellets, manufactured by BASF, Ludwigshafen/Rhein, Germany, were stored at 40°C and 40 Pa (≈0.3 Torr) in a vacuum oven for about two weeks to remove moisture and air. Thereafter they were carefully homogenized in a vented double-screw extruder and worked to rods of circular cross-section (diameter ≈ 3 cm). Rods of suitable length were then compression moulded (20 min preheating at 208°C, 30 min processing at 208°C and 6 MPa, cooling at constant pressure with a rate of 2°C min^{-1}, i.e. the samples were cooled so slowly that they were allowed to anneal during cooling) into sheets of dimensions (0.5–1.5) × (160–240) × 300 mm^3. Visual and polarization optical controls made sure that the subsequently examined sheets were free of bubbles and molecular orientations.

The molar-mass distribution parameters of the pellets and the sheets were determined by means of gel permeation chromatography (h.p.l.c. system with refractive index detector from Knauer, Germany, and PL-Gel column, 5 μm 7.5 × 600 mm, from Polymer Laboratories, UK, operated at 45°C with tetrahydrofuran (THF) at 1.06 ml min^{-1}). The obtained parameters of the PS pellets were:

$$M_n = 102\,000\ \text{g mol}^{-1} \qquad M_w = 293\,000\ \text{g mol}^{-1}$$

$$M_z = 632\,000\ \text{g mol}^{-1} \qquad M_w/M_n = 2.87$$

and the parameters of the PS sheets were:

$$M_n = 96\,500\ \text{g mol}^{-1} \qquad M_w = 237\,000\ \text{g mol}^{-1}$$

$$M_z = 480\,000\ \text{g mol}^{-1} \qquad M_w/M_n = 2.46$$

The relaxation-time spectrum of the subsequently examined PS sheet samples was determined by measuring the frequency dependence of the storage modulus $G'(\omega)$ and the loss modulus $G''(\omega)$ from $\omega = 0.1$ to 100 s^{-1} at several temperatures between 140 and 230°C with a cone–plate rotational shear rheometer (RMS-800 from Rheometrics, USA). The master curves for 140°C, depicted in *Figure 1*, were derived from the measured curves by means of the time–temperature superposition principle[20], and the mechanical relaxation-time spectrum $\{g_m, \tau_m\}$, given in *Table 1*, was derived from the master curves with a procedure described in ref. 21. The temperature dependence of the shift factor, a_T, obtained

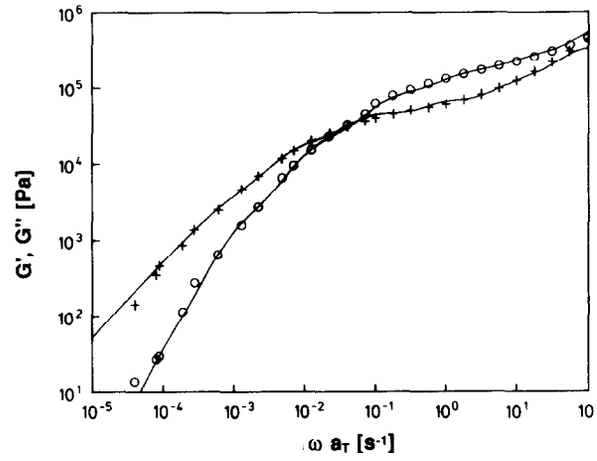

Figure 1 Master curves $G'(\omega)$ and $G''(\omega)$ for PS at 140°C; the abscissa is the reduced circular frequency ωa_T. The symbols are measured data; the curves were calculated from the relaxation-time spectra $\{g_m, \tau_m\}$

Table 1 Discrete relaxation-time spectrum $\{g_m, \tau_m\}$ of the subsequently examined PS at 140°C

m	τ_m (s)	g_m (Pa)	$g_m\tau_m$ (Pa s)
1	10^{-3}	714 000	714
2	10^{-2}	525 000	5 247
3	10^{-1}	119 300	11 930
4	1	85 900	85 900
5	10	66 070	660 700
6	10^2	20 900	2 090 000
7	10^3	2 100	2 108 000
8	10^4	26.8	267 900

by applying the $t-T$ superposition principle, revealed that the activation energy for viscous flow, E_f, is 23 kcal mol^{-1} in the temperature range between 190 and 230°C and 46 kcal mol^{-1} in the lower range between 140 and 180°C. The same result has been reported in ref. 22. It is interesting to note that the change in E_f observed here and also by Dienes and Dexter[22] occurred at a temperature that is about 1.2 times the glass transition temperature in Kelvins. Concerning this fact, it should be mentioned that there is evidence for several polymers that there is an intermolecular liquid–liquid transition at $T_{ll} \approx 1.2 \times T_g$ (ref. 23). For narrow-distribution PS (with $M > 30\,000$) Onogi *et al.*[24] found for a_T the following dependence on temperature (in °C):

$$\log a_T = [-7.14(T - 160)]/[112.1 + (T - 160)]$$

However, if their results are transformed into an $\ln a_T$ vs. $1/T$ plot (T in K) we get $E_f \approx 32$ kcal mol^{-1} for T between 180 and 260°C, and $E_f \approx 72$ kcal mol^{-1} for T between 120 and 180°C.

The rheo-optical apparatus

The experimental equipment consisted of three parts: (i) a stretching apparatus, (ii) a device for thickness control, and (iii) an apparatus for the measurement of optical retardation.

A simpler version of the measuring system, and results from a rheo-optical study of polyisobutylene at room temperature, have already been published[25]. *Figure 2* shows a schematic diagram of the stretching apparatus. The sample (K) was introduced into the thermostatted

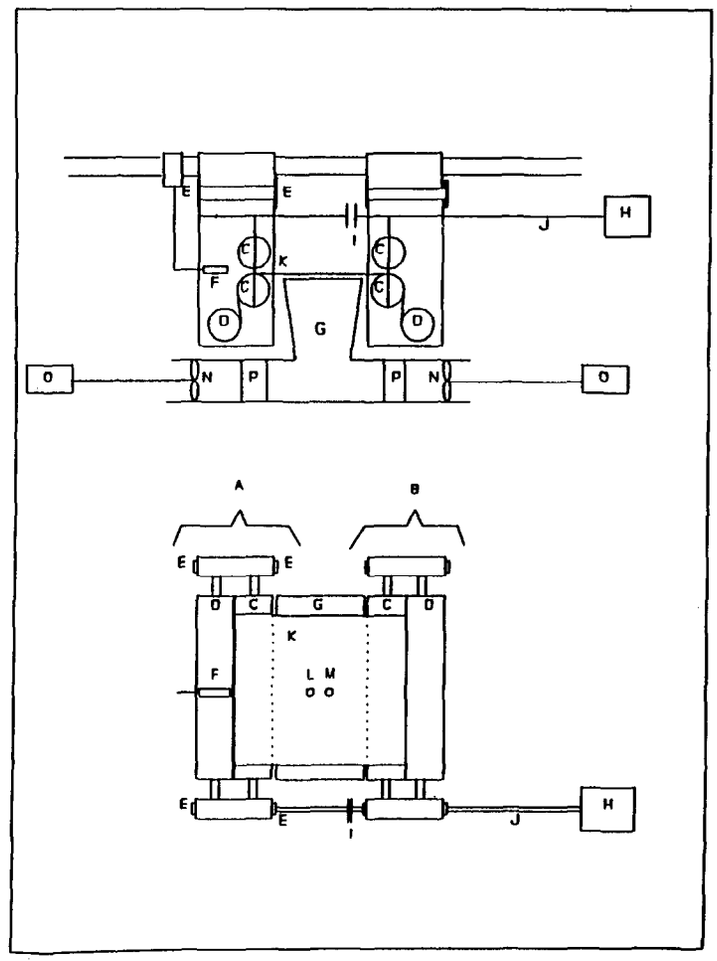

Figure 2 The stretching apparatus: (A) movable clamp, (B) fixed clamp, (C) rotary clamp, (D) cylinder, (E) leaf spring, (F) displacement transducer, (G) funnel, (H) driving motor, (I) membrane, (J) driving axle, (K) sample, (L) light beam for the measurement of the optical retardation, (M) light beam for the measurement of the thickness, (N) ventilator, (O) motor, (P) heating blocks. The sample length between the two pairs of rotary clamps is 200 mm

chamber (not shown here) and fixed by two pairs of rotary clamps (C). Ribbons of textile, which were glued at both ends of the sample, were fixed at the cylinders (D); this ensured that the sample did not wind around the clamps. A finely adjusted gas stream, generated by ventilators (N, O), was blown through the perforated cover plate of the funnel (G), to prevent the sample from sagging under its own weight. When the local and temporal deviations of temperature in the sample were less than ±0.1°C the gas stream was reduced almost to zero and the test was started immediately (usually ca. 30 min after the insertion of the sample; during this time the sample was allowed to anneal further). At the beginning of each test the optical retardation of the sample was 0 ± 0.5 nm (i.e. the initial Δn was $0 \pm 3 \times 10^{-7}$–10^{-6}). Applying a constant rotational speed to the clamps at $t = 0$ produced elongation with constant derivative of the Hencky strain $\dot{\epsilon}_I = \dot{\epsilon}_0 h(t)$ (ref. 12). The resulting tensile force deflected the leaf springs (E); the corresponding shift of the clamp pair (A) from the initial position was measured with a linear displacement transducer (F). To allow the clamp pair (A) to move, the driving axle (J) was axially decoupled by a special membrane (I). Reducing the driving speed of the clamps according to the function $\dot{\lambda}/(1 + \dot{\lambda}t)$ produced elongations with constant stretch rate $\dot{\lambda}_I = \dot{\lambda}_0 h(t)$. In this mode of operation the motor (H) was controlled by a feedback mechanism, which is described in ref. 26.

The change of the thickness of the sample, $d(t)$, was monitored with a two-frequency absorptiometer, the construction and principle of measurement of which are described in ref. 27. For the PS samples the thickness was determined by simultaneous measurement of the absorbance at 1659 nm (where PS shows an overtone absorption band) and at 1500 nm (where PS is free of absorption). The calibration of the instrument was performed by measuring the absorbances of a series of samples covering the thickness range from 0.1 to 2 mm at several elevated temperatures. For these measurements, the samples were placed in a vessel filled with Fomblin (Montedison, Milano, Italy). The thickness at elevated temperatures was calculated from the coefficient of thermal expansion[28] and from the room-temperature thickness, which was measured with a micrometer gauge. After correction of the instrument response for the absorbance of the glass vessel and the Fomblin, a linear regression between absorbance and thickness provided the calibration factor. In order to make sure that the thickness measurements during elongation were not affected by dichroic effects, the absorbances in a solid anisotropic sample were measured parallel and perpendicular to the draw direction. For

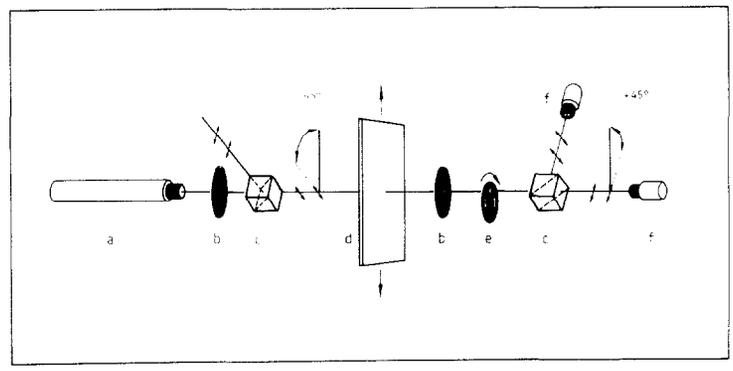

Figure 3 The apparatus for the measurement of the optical retardation: (a) He–Ne laser with collimating beam expander, (b) iris diaphragm, (c) polarizing beam-splitter cube, (d) sample and stretch direction, (e) chopper wheel with retardation plate, (f) detector with collecting lens

this purpose a near-infra-red polarizer (model 27360, LOT, Darmstadt, Germany) was mounted at the position of maximum transmission in a spectrometer (Lambda 9, Perkin–Elmer, USA) and the sample was rotated. This procedure ensured that the measured dichroic ratio was not influenced by instrument polarization due to mirrors and gratings. At both the reference and measuring wavelength there was no dichroism detected. This verified that the thickness measurements were not affected by the state of orientation of the sample.

Figure 3 shows the apparatus for the measurement of the optical retardation, $\Gamma(t)$. A He–Ne laser (a) (model 3025H-PH, Hughes Aircraft, USA) was used as monochromatic light source ($\lambda = 632.8$ nm). A polarizing beam splitter cube (c) produced a linearly polarized beam vibrating in a plane that was inclined by 45° to the direction of the applied stretch. In the deformed sample (d), the incident linearly polarized beam was split into an ordinary and an extraordinary ray (vibrating with the light vector parallel and perpendicular, respectively, to the draw direction), which were both linearly polarized, too, but perpendicular to one another and propagating through the sample with different velocities. A sample of thickness d produced an optical retardation of $\Gamma = \Delta nd$, where $\Delta n = n_{\parallel} - n_{\perp}$. A second polarizing beam splitter cube separated the light emerging from the sample into two components, one vibrating in the same plane as the incident ray, the other perpendicular to it. The intensities of these beams, $I_{\parallel}$ and $I_{\perp}$ (here $\parallel$ and $\perp$ relate the plane of polarization of the emerging light to that of the incident light, whereas in Δn they are related to the draw direction of the sample), were measured simultaneously by two photodiodes (f). The output of each of these was shaped into a rectangular signal by means of a rotating chopper disc (e), which periodically interrupted the emergent beams. If the intensity of all radiation emerging from the sample is designated by I_0, then the observed intensities $I_{\parallel}$ and $I_{\perp}$ are[29]:

$$I_{\parallel} = I_0 \cos^2(\pi\Gamma/d) \tag{7a}$$

$$I_{\perp} = I_0 \sin^2(\pi\Gamma/d) \tag{7b}$$

As the signals of the two photodiodes are complementary, i.e.

$$I_{\parallel} + I_{\perp} = I_0 \tag{8}$$

there is no need for calibration. The optical retardation Γ can be derived directly from the measured quantities, $I_{\parallel}$ and $I_{\perp}$:

$$\Gamma = (\lambda/\pi)\arcsin[I_{\perp}/(I_{\parallel} + I_{\perp})]^{1/2} \tag{9}$$

The insertion of a quartz plate into the chopping disc (e), which periodically added a further retardation of $\Gamma_q \approx -\lambda/4$ to the retardation of the sample, provided two major advantages. It allowed determination of (i) the sign of Γ, and (ii) the absolute value of Γ. The accuracy of the instrument was checked by means of a Soleil–Babinet compensator (model RKQ 12, calibrated for $\lambda = 632.8$ nm; B. Halle Nachf., Berlin).

Experimental procedure

During each experiment the thickness $d(t)$, the rim force $F(t)$ and the optical retardation $\Gamma(t)$ were measured at a rate of ca. $30\,s^{-1}$, and the width of the sample $b(t)$ was monitored photographically at a rate of ca. $3\,s^{-1}$. The quantities $d(t)$, $F(t)$ and $\Gamma(t)$ were digitized by means of an A–D converter (Dash 16, MetraByte, USA) and fed into a personal computer (PC, IBM-AT, USA). The data acquisition programs are detailed in ref. 26. The recorded data were used for further computation only until a time for which a homogeneous deformation was guaranteed. The actual tensile stress $\sigma(t)$ was derived from $d(t)$, $F(t)$ and $b(t)$:

$$\sigma(t) = F(t)/[d(t)b(t)] \tag{10}$$

The optical retardation and the thickness provided the actual birefringence:

$$\Delta n(t) = \Gamma(t)/d(t) \tag{11}$$

and the stress-optical coefficient C was obtained as given by equation (6):

$$C = \Delta n(t)/\sigma(t)$$

Errors

The errors of the measured quantities were determined according to standard procedures[30]. The obtained results for the quantities of interest are compiled in *Table 2*.

RESULTS

The effect of sample dimensions

The decrease of the thickness $d(t)$ and the width $b(t)$ of

Table 2 Relative errors of the quantities of interest

Quantity	Relative error (%)
Tensile stress	≤ 3.5
Birefringence	≤ 1.5
Stress-optical coefficient	≤ 4.0

Table 3 The dependence of c_{Hb} on $\dot{\epsilon}$

$\dot{\epsilon}$ (s^{-1})	b_0 (mm)	$c_{Hb}(t)$ (s^{-2})
1.27	138	$(89 \pm 6) \times 10^{-3}$
0.31	128	$(3.4 \pm 0.3) \times 10^{-3}$
0.05	120	$< 10^{-5}$

Table 4 The dependence of c_{Sb} on $\dot{\lambda}$

$\dot{\lambda}$ (s^{-1})	b_0 (mm)	$c_{Sb}(t)$ (s^{-2})
1.39	136	$(14 \pm 1) \times 10^{-3}$
0.50	141	$(4 \pm 0.2) \times 10^{-3}$
0.11	140	$(0.3 \pm 0.015) \times 10^{-3}$

an incompressible fluid during simple elongation is:

$$b(t) = b_0/(\lambda_I)^{1/2} \tag{12}$$

$$d(t) = d_0/(\lambda_I)^{1/2} \tag{13}$$

However, the results of measurement at 140°C showed that $b(t)$ generally (i.e. when the initial width b_0 was larger than 80 mm or when the strain rate was not very small) decreased slower and $d(t)$ decreased faster than expected. In a test with $\dot{\epsilon}_0 = \text{const.}$ the actual deformation was:

$$\ln[b(t)/b_0] = \ln \lambda_{II} = -0.5\dot{\epsilon}_0 t + c_{Hb}(t)t^2 \tag{14}$$

$$\ln[d(t)/d_0] = \ln \lambda_{III} = -0.5\dot{\epsilon}_0 t - c_{Hd}(t)t^2 \tag{15}$$

where $c_{Hb} = c_{Hd}$. The deformation in draw direction, $\lambda_I = \exp(\dot{\epsilon}_0 t)$, derived from photographs (taken on samples that were marked with a grid pattern) deviated at maximum by 2% from λ_I calculated with equations (14) and (15). This proved that the elongations were indeed performed with $\dot{\epsilon}_0 = \text{const.}$ and that the investigated melt behaved as an incompressible fluid (i.e. $\ln \lambda_I + \ln \lambda_{II} + \ln \lambda_{III} = 0$).

In a test with $\dot{\lambda}_0 = \text{const.}$ the deformation was:

$$[b_0/b(t)]^2 = (\lambda_{II})^{-2} = 1 + \dot{\lambda}_0 t - c_{Sb}(t)t^2 \tag{16}$$

$$[d_0/d(t)]^2 = (\lambda_{III})^{-2} = 1 + \dot{\lambda}_0 t + c_{Sd}(t)t^2 \tag{17}$$

The plot of $[b_0 d_0/b(t)d(t)]$ vs. time verified that the deformation in draw direction, λ_I, was a linear function of time: $\lambda_I = 1 + \dot{\lambda}_0 t$.

The values of the deviation parameters, $c_{Hb}(t)$ and $c_{Sb}(t)$, for different elongational rates are given in *Tables 3* and *4*. The nature of the actual elongations can easily be visualized by means of the ratios $m_\epsilon = \dot{\epsilon}_{II}/\dot{\epsilon}_I$ and $m_\lambda = \ln \lambda_{II}/\ln \lambda_I$. In the elongations presented, m_ϵ and m_λ were:

$$m_\epsilon(t) = -0.5 + 2c_{Hb}t/\dot{\epsilon}_0 \tag{18}$$

$$m_\lambda(t) = -0.5[\ln(1 + \dot{\lambda}_0 t - c_{Sb}t^2)/\ln(1 + \dot{\lambda}_0 t)] \tag{19}$$

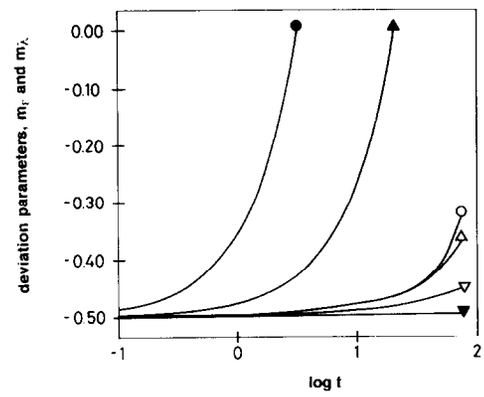

Figure 4 Plot of m_ϵ and m_λ vs. logarithm of duration of deformation: $\dot{\epsilon}_0 = \text{const}$, (●) 1.27 s^{-1}, (▲) 0.31 s^{-1}, (▼) 0.05 s^{-1}; $\dot{\lambda}_0 = \text{const}$, (○) 1.39 s^{-1}, (△) 0.5 s^{-1}, (▽) 0.11 s^{-1}

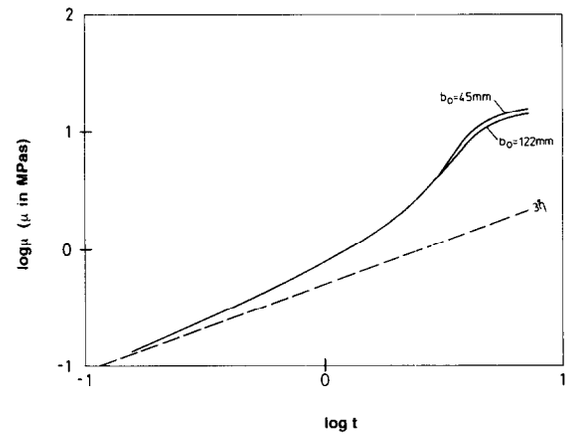

Figure 5 Plot of $\log \mu$ vs. $\log t$ for two samples with different width, both elongated with $\dot{\epsilon}_0 = 0.6\,s^{-1}$ at $T = 140°C$

Figure 4 shows that the change from simple into planar elongation (simple elongation is characterized by $m = -0.5 = \text{const.}$, and planar elongation by $m = 0 = \text{const.}$) which occurred during deformation is strongly dependent on the applied strain rate, $\dot{\epsilon}_0$ and $\dot{\lambda}_0$. It turned out that the deviation from the initial value $m = -0.5$ further depended on: (i) the temperature (at $T = 160°C$ there was no deviation from $m = -0.5$ to observe, even when $\dot{\epsilon}_0$ was 2.4 s^{-1} and b_0 was 140 mm), and (ii) the ratio of the initial width and length of the sample, L_0/b_0 (L_0 is the fixed distance between the two pairs of rotary clamps, i.e. 200 mm). However, when $L_0/b_0 > 2.5$, the dependence of m on b_0 was negligible.

The thickness of the sample (d_0 ranged from 0.5 to 1.5 mm) did not show any effect on m. The dependence of the results of tensile testing of solid samples on the specimen length/width ratio has been investigated by Arridge and Folkes[31]. Their measurements of Young's modulus on highly anisotropic samples of linear polyethylene (along the symmetry axis) showed that end effects due to clamping, i.e. irregular stress distribution, can be neglected, only if $L_0/b_0 > 80$ (at $L_0/b_0 = 20$ the measured modulus was about 60% of the true value at $L_0/b_0 > 80$). This result agrees with our findings at elevated temperatures.

Figure 5 shows how the elongational viscosity, $\mu(t) = \sigma(t)/\dot{\epsilon}_0$, is influenced by $m_\epsilon(t)$. The upper curve

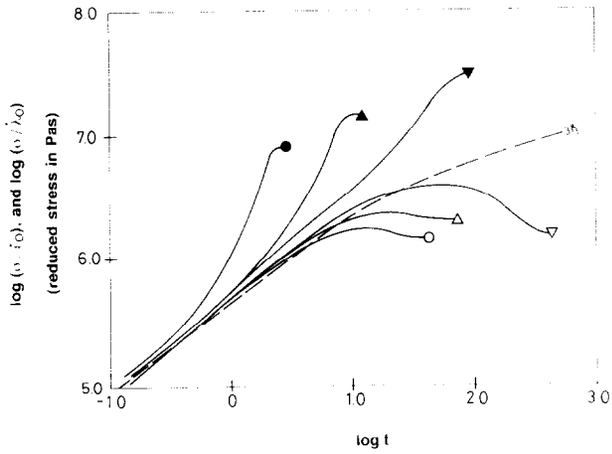

Figure 6 The course of the reduced stress of PS at 140°C in strong and weak flows, $\sigma/\dot{\epsilon}_0$ and $\sigma/\dot{\lambda}_0$, respectively: $\dot{\epsilon}_0$ = const, (●) 1.27 s^{-1}, (▲) 0.31 s^{-1}, (▼) 0.05 s^{-1}; $\dot{\lambda}_0$ = const, (○) 1.39 s^{-1}, (△) 0.5 s^{-1}, (▽) 0.11 s^{-1}

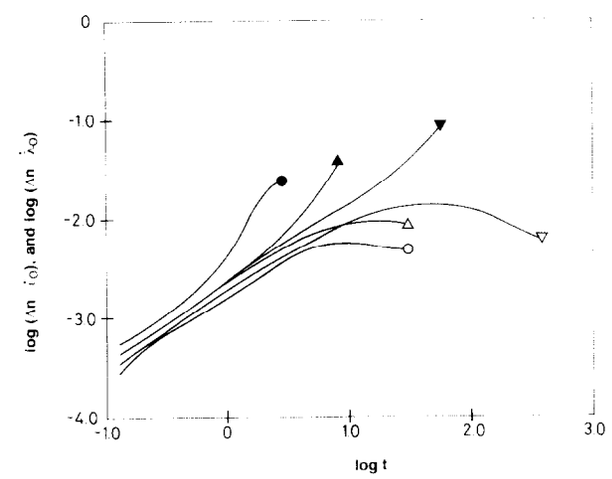

Figure 7 The course of the reduced birefringence of PS at 140°C in strong and weak flows, $\Delta n/\dot{\epsilon}_0$ and $\Delta n/\dot{\lambda}_0$, respectively. The symbols have the same meaning as in *Figure 6*

is from a sample with $L_0/b_0 = 4.4$, m_ϵ = const. = −0.5; the lower curve is from a sample with $L_0/b_0 = 1.6$, $m_\epsilon(t) = -0.5 + 0.08t$. Thus, for $\dot{\epsilon}_0 = 0.6\,s^{-1}$ and $L_0/b_0 = 1.6$, the effect of $m_\epsilon \neq$ const. is appreciable only at $t > 3$ s; the largest deviation from the upper curve occurs at the end and is about 15%. This gives an estimation of the reduction of orientation that resulted from the fact $m_\epsilon = m_\epsilon(t)$.

Reduced stress and reduced birefringence of PS in strong and weak flows

Figure 6 shows the time dependence of the reduced stress for the PS melt during elongation at 140°C with $\dot{\epsilon}_0$ = const. and $\dot{\lambda}_0$ = const., i.e. during strong and weak flows. It is recognized from *Figure 6* that the response of the PS melt in terms of 'hardening' and 'thinning' depends on the mode of the applied deformation. Similar results have been reported by Zülle *et al.*[14] for an LDPE melt at 150°C.

Figure 7 depicts the course of the reduced birefringence, $\Delta n(t)/\dot{\epsilon}_0$ and $\Delta n(t)/\dot{\lambda}_0$, that was recorded simultaneously with the reduced stress.

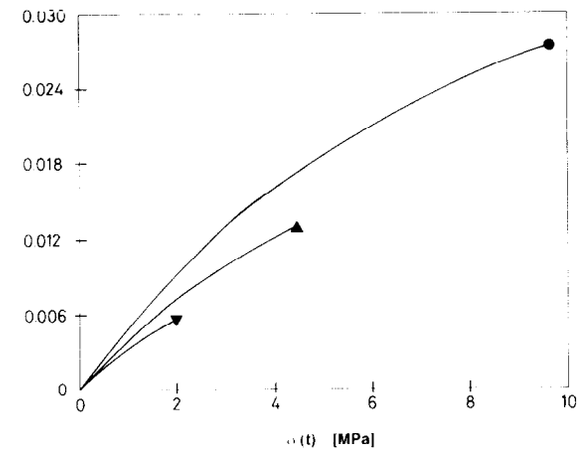

Figure 8 Negative value of Δn vs. σ for three tests at 140°C with $\dot{\epsilon}_0$ = const. The symbols have the same meaning as in *Figure 6*

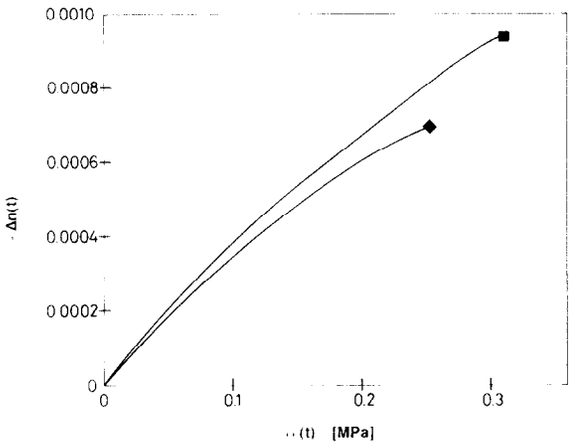

Figure 9 Negative values of Δn vs. σ for two tests at 160°C with $\dot{\epsilon}_0$ = const: (■) 2.4 s^{-1}, (◆) 1.2 s^{-1}

The stress-optical coefficient (SOC) of PS

In *Figure 8* the birefringence $\Delta n(t)$ is plotted vs. the tensile stress $\sigma(t)$ for tests with $\dot{\epsilon}_0$ = const.. At low stress levels the initial value of the stress-optical coefficient, $C = \Delta n(t)/\sigma(t)$, is about -4.5×10^{-9} Pa^{-1}. The deviation from the linear stress-optical rule that occurs at higher stresses is well known. Matsumoto and Bogue[32] observed this deviation on a PS melt ($M_w = 2.8 \times 10^5$, $M_w/M_n = 4.6$, $\dot{\epsilon}_0 = 0.075\,s^{-1}$, $T = 120$ to 157°C) at $\sigma > 1$ MPa; in the lower stress range, however, they obtained a constant *SOC* of -6.1×10^{-9} Pa^{-1}. Similar results for a PS melt ($M_w = 2.5 \times 10^5$, $M_w/M_n = 2.44$, $\dot{\epsilon}_0 = 0.01$ to $0.5\,s^{-1}$, $T = 126$ to 146°C) have also been obtained by Muller and Froelich[33]. They obtained an *SOC* of -4.7×10^{-9} Pa^{-1}, which was constant up to $\sigma \approx 1.5$ MPa. However, *Figure 8* shows a further deviation from the linear stress-optical rule: the *SOC* of the PS investigated here depends on the applied strain rate, too.

Thus, in general, the *SOC* must be written as $C = C(\sigma, \dot{\epsilon}_0)$. It should be emphasized that the same $\dot{\epsilon}_0$ dependence of C was also observed on samples with smaller width (for which m = const.). *Figure 9* shows some results obtained at $T = 160$°C (as already mentioned, at this temperature m = const. = −0.5). In *Figure 10* $\Delta n(t)$ is plotted vs. $\sigma(t)$ for the tests performed

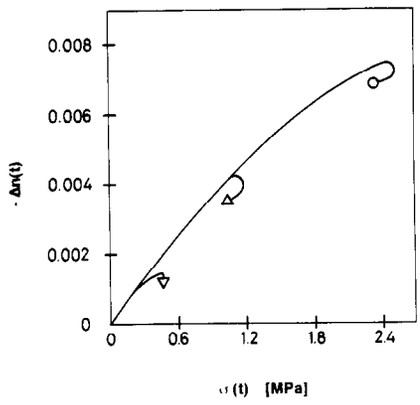

Figure 10 Negative value of Δn vs σ for three tests at 140°C with $\dot{\lambda}_0 = \text{const}$. The symbols have the same meaning as in *Figure 6*

Table 5 Change of the *SOC* of PS during elongation at 140 and 160°C and one-sided compression at 170°C

	$C_{in} \times 10^9$ (Pa^{-1})	$C_{fin} \times 10^9$ (Pa^{-1})
$T = 140°C$		
$\dot{\epsilon}_0 = 0.05$	−4.5	−2.9
$\dot{\epsilon}_0 = 1.2$	−4.5	−2.8
$\dot{\lambda}_0 = 0.11$	−5	−2.8
$\dot{\lambda}_0 = 1.39$	−5	−3.1
$T = 160°C$		
$\dot{\epsilon}_0 = 0.9$	−4	−3.3
$\dot{\epsilon}_0 = 2.4$	−4	−3.2
$T = 170°C$		
$\dot{\epsilon}_0 = -0.0187$	−2.5	−3.6
$\dot{\epsilon}_0 = -0.31$	−1.5	−3.6

with $\dot{\lambda}_0 = \text{const}$.. Here, in weak flows, $\Delta n(t)$ and $\sigma(t)$ are not monotonically increasing for all times. Both functions increase to a maximum; however, the maximum of $\Delta n(t)$ occurs sooner than that of $\sigma(t)$, and after the maximum, the birefringence decreases faster than the tensile stress. Therefore, in weak flows, the relation between $\Delta n(t)$ and $\sigma(t)$ is no longer a unique function. Such a non-unique relationship between $\Delta n(t)$ and pressure $-\sigma(t)$ has already been observed on a PS melt ($M_w = 2.4 \times 10^5$, $M_w/M_n = 2.76$, $T = 170°C$) in one-sided compression (with $\dot{\epsilon}_0 = \text{const}$. ranging from -0.0187 to $-0.31\,s^{-1}$; the highest pressure was only about 0.07 MPa) by Van Aken and Janeschitz-Kriegl[34]. They determined $\Delta n(t)$ and $-\sigma(t)$ during build-up, steady state and relaxation of the flow. In the build-up phase the *SOC* was found to have a very strong dependence on the pressure and $\dot{\epsilon}_0$. However, the steady-state and the relaxation data gave a constant *SOC* of -3.6×10^{-9} and $-4 \times 10^{-9}\,Pa^{-1}$, respectively. The change of the *SOC* during the fastest and the slowest compression reported in ref. 34 and during some elongations reported here are compiled in *Table 5*. The table clearly shows that the *SOC* of PS changed markedly during these experiments, and it is most interesting that its absolute value increases during one-sided compression (i.e. when $\dot{\epsilon}_0 < 0$), whereas it decreases during elongation (i.e. when $\dot{\epsilon}_0 > 0$). Thus, in general, the *SOC* of PS has to be written as: $C = C(\dot{\epsilon}_0, t)$. *Figure 11* shows the time dependence of the *SOC* during the two slowest elongations (i.e. with $\dot{\epsilon}_0 = \text{const.} = 0.05$ and $\dot{\lambda}_0 = \text{const.} = 0.11\,s^{-1}$, respectively) in which the PS

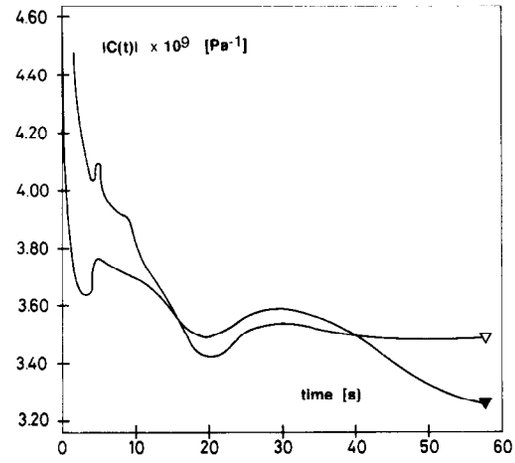

Figure 11 The course of the absolute value of the stress-optical coefficient of PS elongated at 140°C with $\dot{\epsilon}_0 = \text{const} = 0.05\,s^{-1}$ (▼) and $\dot{\lambda}_0 = \text{const} = 0.11\,s^{-1}$ (▽)

melt behaved linear-viscoelastically until $t \approx 5$ s. This plot clearly demonstrates that the *SOC* of the PS melt investigated here is also a time-dependent function in the linear viscoelastic range of deformation. In both tests, i.e. during elongation with $\dot{\epsilon}_0 = \text{const.}$ and $\dot{\lambda}_0 = \text{const.}$, the *SOC* decreases. However, the decrease of $|C(t)|$ is not monotonic; both curves pass through several local minima and maxima. It should be emphasized that we believe these extrema to be real, i.e. not to be artefacts. A minimum in $|C|$ can also be derived from the elongation with $\dot{\lambda}_0 = 1.39\,s^{-1}$ (see *Figure 10*); at $\sigma \approx 2.45$ MPa, i.e. shortly after the stress has reached its maximum value (of ca. 2.5 MPa), C is ca. $-2.8 \times 10^{-9}\,Pa^{-1}$ which is definitely lower than the final value of $-3.1 \times 10^{-9}\,Pa^{-1}$.

DISCUSSION

It is generally agreed that the birefringence of any polymer is always composed of two different contributions[35,36]:

$$\Delta n = \Delta n^d + \Delta n^o \tag{20}$$

The distortional birefringence, Δn^d, is associated with elastic deformation of bonds and valence angles (leading to an increase of internal energy), and Δn^o, the orientation birefringence, is related to orientation of optically anisotropic structural units (which leads to a decrease of entropy). At temperatures well below T_g, where the chain segment mobility is strongly reduced, the measured birefringence is governed by Δn^d, while at high temperatures (i.e. near or above T_g) Δn^o is dominant. The two contributions differ significantly with regard to the relaxation time, i.e. Δn^d relaxes by orders of magnitude faster than Δn^o. Furthermore, in the case of PS, Δn^d is of positive sign and is relatively small compared to Δn^o, which is of negative sign: $\Delta n^d/\sigma \approx 10^{-11}\,Pa^{-1}$ and $\Delta n^o/\sigma \approx -5 \times 10^{-9}\,Pa^{-1}$ (ref. 37). On the other hand, the tensile stress can also be divided into an energy and an entropy elastic part:

$$\sigma = \sigma_u + \sigma_s \tag{21}$$

Thus, upon relaxation of the energy elastic part of deformation, the absolute value of the *SOC* of PS is increasing. Such observations have been reported by Retting[38] for a PS melt ($M_w \approx 4 \times 10^5$, $M_w/M_n \approx 2.5$–

3.0). During elongation ($\dot{\lambda}_0 = 0.01\,s^{-1}$, $T = 110$ to 140°C), Retting observed that the ratio $|\Delta n(t)|/\sigma(t)$ of PS increased right from the beginning of deformation until it gradually reached a constant final value, which was between -4.4×10^{-9} and $-5 \times 10^{-9}\,Pa^{-1}$. At 110°C the final value was obtained after ≈ 100 s, at 120°C after ≈ 15 s, and at 130 to 140°C after ≈ 5 s.

However, a decreasing $|C(t)|$, as shown in *Figures 8* to *11*, cannot be explained this way. We consider these findings as proof that Δn° and σ_s build up and relax by different mechanisms. For the linear viscoelastic range of deformation an increasing and a decreasing *SOC* can be explained by the kinetic orientation model (KOM), which was recently presented by Hoppler and Tomka[19], and also by the phenomenological theory of simple incompressible fluids with fading memory[17]. The phenomenological theory and the kinetic orientation model both provide a constant *SOC* only in two limiting cases, which are in terms of the model[19]:

$$\lim_{t \to 0} C(t) = c \sum (f_i/\tau_i^*) \Big/ \sum g_m = \text{const.} = C_{in} \qquad (22)$$

$$\lim_{t \to \infty} C(t) = c \sum f_i \Big/ \sum g_m \tau_m = \text{const.} = C_{fin} \qquad (23)$$

Here τ_i^* is an optical relaxation time, $c = \pi(n_0^2 + 2)^2/9RTn_0$ is a constant (n_0 is the refractive index of the undeformed, isotropic melt; R is the gas constant) and $f_i = p_i a_i \Delta\alpha_{il}/[1 + \cosh(\Delta G_i/RT)]$ is a constant weighting factor (in $J\,s\,mol^{-1}$; p_i, a_{il}, $\Delta\alpha_{il}$ and ΔG_i are model quantities). From equations (22) and (23) it is evident that a constant *SOC* can only occur if $C_{in} = C_{fin}$. Therefore, the conditions for $C = \text{const.}$ are:

(i) The mechanical relaxation-time spectrum, $\{g_m, \tau_m\}$, has the same number of values as the optical relaxation-time spectrum, $\{(cf_i/\tau_i^*), \tau_i^*\}$.
(ii) Each τ_m is equal to the corresponding τ_i^*.
(iii) Each g_m is related by the same constant to the corresponding optical quantity (cf_i/τ_i^*).

If all of these conditions are fulfilled, then we can write the *SOC* as a constant, which in terms of the microscopic model (KOM) is:

$$C = \text{const.} = (cf_i/\tau_i^*)/g_m \qquad (24)$$

As the above-mentioned conditions cannot be derived from any theory, we have to admit the case $C_{in} \neq C_{fin}$, which means that there is an intermediary change of the *SOC*. In a previous paper[19] Hoppler and Tomka have shown that the time dependence of the *SOC* may be of any kind; it may even be very weak (if there is a high similarity between the mechanical and the optical relaxation-time spectrum), and it vanishes completely when the time is about twice the highest relaxation time.

So far the time dependence of the *SOC* has only been discussed with regard to PS. However, there is experimental evidence that points out that the *SOC* of any polymer with optically anisotropic side groups is a time-dependent function. In a dynamic rheo-optical study, Read[16] subjected samples of poly(methyl acrylate) (PMA, $T_g \approx 10$°C) to a sinusoidal strain with small amplitude. The measurements (amplitudes and relative phases of the stress, strain and birefringence) were made in the frequency range 1 to $20\,s^{-1}$ and temperature range 16.6 to 61.5°C. From the results of measurement, master curves with an extended frequency range (≈ 20 to $\approx 10^8\,s^{-1}$) were constructed. For $T = 61.5$°C the ratio of the amplitudes of the stress and the birefringence, the phase angle by which the birefringence leads the stress, and also the real and imaginary components of the complex stress-optical coefficient all exhibited a very pronounced frequency dependence. If the *SOC* of PMA was a constant then the stress and the birefringence would be in phase and the ratio of their amplitudes would be independent of frequency, and in the complex representation the real part of C would be independent of frequency and the imaginary part of C would be zero. Thus, the results found by Read[16] indicate that the *SOC* of PMA would be a time-dependent function in a static experiment (e.g. in a linear viscoelastic elongation with $\dot{\epsilon}_0 = \text{const.}$).

Furthermore, the violation of the stress-optical rule has also been observed on dilute polymer solutions subject to extensional flow[39–41]. Therefore, it seems that the simple rule that has been found to be valid for many polymeric liquids under simple shear breaks down in extensional flow. The question arises also whether and how the observed phenomenon is influenced by the molecular-weight distribution of the sample.

CONCLUSIONS

The stress-optical rule[8,15], which considers the *SOC* of a polymer melt as a time- and strain-independent constant, is not confirmed by the present study. In contrast, this study shows that the *SOC* of the PS investigated here depends on the time and the strain rate. It is most likely that any polymer melt having a structure with optically anisotropic side groups (as e.g. PMA and PMMA) would behave similarly to the PS melt of this study. Information on transient stresses in polymer melts can thus only be derived from optical measurements if the time and the strain-rate dependence of the *SOC* is known, or alternatively if it is verified that the *SOC* is constant.

Concerning the linear viscoelastic range of deformation, the results of this study confirm the predictions of the kinetic orientation model (KOM), which was recently presented[19], as well as those of the phenomenological theory of simple incompressible fluids with fading memory[17]. According to the KOM the time dependence of the *SOC* in the linear range is associated with differences between the mechanical and optical relaxation-time spectrum.

The set-up of molecular orientation during elongational flows (measured as birefringence, Δn) depends strongly on the deformation history and on the duration of the flow. Elongations carried out with $\dot{\epsilon} = \text{const.}$ (i.e. with exponentially increasing stretch ratio $\lambda = \exp(\dot{\epsilon}t)$) provide a strong anisotropy, i.e. in strong flows the response of the melt is 'hardening'; $\Delta n(t)$ increases steadily. During elongations with $\dot{\lambda} = \text{const.}$ (i.e. with linearly increasing stretch ratio), the optical anisotropy is weak, i.e. in weak flows the response of the melt is 'thinning'; $\Delta n(t)$ passes through a comparatively small maximum and thereafter decreases steadily. Concerning the elongational viscosity, similar results have previously been reported by Zülle *et al.*[14].

For the correct interpretation of rheological test results, it is very important that the deformation history and the homogeneity of the deformation are checked carefully. In our case, the checks were performed by simultaneous recording of the width and the thickness of the samples during deformation. The results of these measurements demonstrated that the true and the pregiven deformation may deviate significantly from one another.

ACKNOWLEDGEMENTS

The authors wish to express their gratitude to Professor J. Meissner and Dr H. Hürlimann for valuable discussions, and to the Swiss National Foundation for Scientific Research (Grant No. 5.521.330.842/2) for financial support.

REFERENCES

1 Hermans, P. H. 'Contributions to the Physics of Cellulose Fibres', Elsevier, Amsterdam, 1946
2 Ward, I. M. (Ed) 'Structure and Properties of Oriented Polymers', Applied Science, London, 1975
3 Hellmuth, W., Kilian, H.-G. and Müller, F. H. *Kolloid Z. Z. Polym.* 1967, **218**, 10
4 Jasse, B. and Koenig, J. L. *J. Polym. Sci., Polym. Phys. Edn.* 1979, **17**, 799
5 Jones, T. T. *Pure Appl. Chem.* 1976, **45**, 40
6 Lefebvre, D., Jasse, B. and Monnerie, L. *Polymer* 1982, **23**, 706
7 Milagin, M. F., Gabaraeva, A. D. and Shishkin, I. I. *Polym. Sci. USSR* 1970, **12**, 577
8 Janeschitz–Kriegl, H. 'Polymer Melt Rheology and Flow Birefringence', Springer–Verlag, Berlin, 1983
9 Boundry, R. H. and Boyer, R. F. (Eds.) 'Styrene, Its Polymers, Copolymers and Derivatives', Reinhold, New York, 1952
10 Petrie, C. J. S. 'Elongational Flows', Pitman, London, 1979
11 Jaffé, H. H. and Orchin, M. 'Symmetry in Chemistry', Wiley, New York, 1965
12 Meissner, J. *Rheol. Acta* 1969, **8**, 78
13 Meissner, J., Raible, T. and Stephenson, S. E. *J. Rheol.* 1981, **25**, 1, 673
14 Zülle, B., Linster, J. J., Meissner, J. and Hürlimann, H. P. *J. Rheol.* 1987, **31**, 583
15 White, J. L. and Spruiell, J. E. *Polym. Eng. Sci.* 1983, **23**, 247
16 Read, B. E. *Polymer* 1964, **5**, 1
17 Coleman, B. D., Dill, E. H. and Toupin, R. A. *Arch. Rat. Mech. Anal.* 1970, **39**, 358
18 Dill, E. H. *J. Polym. Sci. (C) Polym. Symp.* 1964, **5**, 67
19 Hoppler, H. U. and Tomka, I. *Polymer* 1993, **34**, 2575
20 Ferry, J. D. 'Viscoelastic Properties of Polymers', 3rd Edn., Wiley, New York, 1980
21 Demarmels, A. and Meissner, J. *J. Colloid Polym. Sci.* 1986, **264**, 829
22 Dienes, G. J. and Dexter, F. D. *J. Colloid Sci.* 1948, **3**, 181; Spencer, R. S. and Dillon, R. E. *J. Colloid Sci.* 1948, **3**, 163
23 Enns, J. B. and Boyer, R. F. 'Order in the Amorphous State of Polymers' (Eds S. E. Keinath, R. L. Miller and J. K. Rieke), Plenum, New York, 1987
24 Onogi, S., Masuda, T. and Kitagawa, K. *Macromolecules* 1970, **3**, 109
25 Dinkel, A., Hoppler, H. U., Tomka, I. and Vancso, G. *Angew. Makromol. Chem.* 1987, **153**, 135
26 Dinkel, A. Dissertation, ETH Zürich, No. 9640, 1992
27 Hoppler, H. U. and Tomka, I. *Kunststoffe* 1987, **77**, 162
28 Zoller, P., Bolli, P., Hersche, E. and Foppa, U. *Kunststoffe* 1976, **66**, 363
29 Born, M. and Wolf, E. 'Principles of Optics', Pergamon, Oxford, 1980
30 Hoppler, H. U. Dissertation, ETH Zürich, No. 9099, 1990
31 Arridge, R. G. C. and Folkes, M. J. *Polymer* 1976, **17**, 495
32 Matsumoto, T. and Bogue, D. C. *J. Polym. Sci., Polym. Phys. Edn.* 1977, **15**, 1663
33 Muller, R. and Froelich, D. *Polymer* 1985, **26**, 1477
34 Van Aken, J. A. and Janeschitz–Kriegl, H. *Rheol. Acta* 1981, **20**, 419
35 Stuart, H. A. 'Die Physik der Hochpolymeren', Vol. III (Ed. H. A. Stuart), Springer–Verlag, Berlin, 1955
36 Rudd, J. F. and Gurnee, E. F. *J. Polym. Sci. (A)* 1963, **1**, 2857
37 Stein, R. S. 'Die Physik der Hochpolymeren', Vol. IV (Ed. H. A. Stuart), Springer–Verlag, Berlin, 1956
38 Retting, W. *Colloid Polym. Sci.* 1979, **257**, 689
39 Fuller, G. G. *Annu. Rev. Fluid Mech.* 1990, **22**, 387
40 Talbott, W. H. and Goddard, J. D. *Rheol. Acta* 1979, **18**, 505
41 Fuller, G. G. and Leal, L. G. *Rheol. Acta* 1980, **19**, 580